Alertness-related differences in CF strategy among truck drivers based on naturalistic driving data

Yang Liu[a], Zhijie Yi[a], Boyu Jin[b], Dengbo He[a,b,c,*] and Weiyin Xie[b]

[a]Intelligent Transportation Thrust, The Hong Kong University of Science and Technology (Guangzhou), Guangzhou, 511453, Guangdong, China
[b]Robotics and Autonomous Systems Thrust, The Hong Kong University of Science and Technology (Guangzhou), Guangzhou, 511453, Guangdong, China
[c]HKUST Shenzhen-Hong Kong Collaborative Innovation Research Institute, shenzhen, 518045, Guangdong, China

ARTICLE INFO

Keywords:
Driver alertness
Car-following behavior
Naturalistic driving data
Intelligent Driver Model
DS-HDP-HMM

ABSTRACT

Driver drowsiness is a major safety concern in heavy-duty truck operation, particularly in freeway car-following (CF) scenarios that require prolonged vigilance and continuous longitudinal control. However, how drowsiness-induced reduced alertness influences truck drivers' CF behavior in real-world settings remains insufficiently understood. To address this gap, this study established a naturalistic heavy-truck CF dataset from long-haul freeway operations, with driver alertness labels obtained from a Smart Eye system. A three-level analytical framework was adopted to examine the effects of alertness on CF behavior from the perspectives of high-level behavioral indicators, model-based mechanism characterization, and primitive-level temporal structure. Specifically, overall CF performance was first described using commonly used indicators, then parameterized using the Intelligent Driver Model (IDM), and further interpreted at a finer temporal scale through behavioral primitives identified by a disentangled sticky hierarchical Dirichlet process hidden Markov model (DS-HDP-HMM). The results consistently showed that reduced alertness was associated with changes in drivers' longitudinal adjustment patterns, which may partly reflect compensatory responses. Compared with alert driving, non-alert driving was associated with a more conservative spacing strategy, milder and less aggressive longitudinal regulation, and more near-constant and weak-regulation behavioral primitives, while active acceleration and deceleration corrections were less frequent. These findings provide a multi-level understanding of the longitudinal control mechanisms underlying non-alert truck driving in freeway environments and offer behavioral evidence for the development of intelligent driving assistance systems that can better respond to non-alert road truck drivers.

1. Introduction

Road freight transportation with heavy trucks plays a vital role in modern society. At the same time, however, crashes involving heavy trucks often lead to more severe outcomes due to their large vehicle mass and long braking distance (Chang and Mannering, 1999; Zainuddin et al., 2023). As a result, heavy-truck safety has remained a major concern in road traffic safety. What is more alarming, compared with passenger-car driving, truck driving is typically characterized by longer driving duration, higher workload, more monotonous operating environments, and stronger time-related constraints, making drivers more susceptible to drowsiness and functional degradation during prolonged and demanding transport tasks (Mabry et al., 2022; Casey et al., 2024; McCartt et al., 2000). Drowsiness not only impairs drivers' perception, judgment, and decision-making in response to the traffic environment, but also reduces alertness, delays reactions, worsens operational stability, and weakens risk-response capacity, thereby increasing the likelihood of crashes (Duffy et al., 2015).

At the same time, for truck drivers, operating conditions are primarily concentrated on freeways and arterial corridors, where the driving task typically involves prolonged lane-keeping and continuous following of a lead vehicle (LV) (Ramsay, 2006). Thus, in real-world freight operations, the car-following (CF) is one of the most common and fundamental driving states (Hussain et al., 2025). Compared with short-duration maneuvers, such as overtaking, lane changing, and turning, CF is characterized by longer task duration and relatively simple control demands, while still requiring sustained attention (Zhang et al., 2019). These features make it a typical traffic scenario in which the effects of driver drowsiness are more likely to accumulate and become manifested (Casey et al., 2024).

*Corresponding author
dengbohe@hkust-gz.edu.cn (D. He)
ORCID(s): 0000-0003-4359-4083 (D. He)

Although both driver drowsiness and CF behavior have been widely investigated, there is still a gap in understanding how a low level of alertness, as a result of drowsiness, influences drivers' CF strategies, speed regulation patterns, and spacing preferences, especially among truck drivers in long-haul driving (Mahajan and Velaga, 2021; Zhang et al., 2016). Though a few studies have investigated how differences in alertness may affect drivers' CF behaviors, i.e., the longitudinal vehicle control in response to speed variations in LVs, they were mostly conducted in driving simulators (Afghari et al., 2022; Mahajan and Velaga, 2021), with relatively short experimental durations (Zhang et al., 2016; Tomson et al., 2025). Thus, they provided limited empirical evidence on truck drivers' strategies to cope with low levels of alertness in real-world scenarios, as drivers may have biased speed and gap perception in driving simulators and may self-adjust their strategies in long-distance driving. In summary, previous studies have primarily examined drowsiness-related changes in general driving performance or a limited set of macroscopic CF measures, mostly in passenger-car simulators. Consequently, it remains unclear whether and how reduced alertness as a result of drowsiness changes heavy-truck drivers' overall spacing and speed-regulation strategies, model-represented longitudinal interaction characteristics, and the temporal organization and persistence of specific CF states. Addressing these questions is important not only for understanding drowsiness-related behavioral adaptation in heavy-truck CF, but also for identifying interpretable CF features that may support subsequent driver-state prediction.

To address the aforementioned research gap, as illustrated in Fig. 1, we collected and published a heavy-truck CF dataset from a naturalistic driving study conducted in freeway scenarios, with driver alertness labels obtained based on the percentage of eyelid closure over the pupil over time (PERCLOS) metric (Grace and Steward, 2001). Then, the analysis was conducted at three levels, namely high-level behavioral representation, mechanism-oriented behavioral characterization, and microscopic temporal structure analysis, to provide a comprehensive understanding of the behavioral evolution and potential safety risks of non-alert truck driving in freeway CF scenarios. Specifically, high-level behavioral indicators were first used to characterize the overall changes in CF behavior under a low level of alertness (Vogel, 2003a). Next, given that these high-level indicators mainly reflect behavioral outcomes and provide limited insight into the underlying control mechanisms, the Intelligent Driver Model (IDM) (Treiber et al., 2000) was further employed to parameterize the CF process and to examine the effects of low alertness on drivers' longitudinal control characteristics from a mechanistic perspective (Kesting et al., 2010). Finally, we further investigated the primitive-level temporal structure of driving behavior by employing the hidden Markov model (HMM). Specifically, the Dirichlet process hidden Markov model (DS-HDP-HMM) (Zhou et al., 2020) was selected to model behavioral organization and state transition patterns. This last step, on top of the high-level behavioral indicators and the control mechanisms of CF behaviors that evaluate CF behaviors from a static view, models CF behaviors at a finer temporal scale by answering how CF behavior evolves dynamically over time within a CF segment.

2. Literature review

2.1. Effects of degraded alertness in driving

Compared with the extensive attention devoted to drowsiness detection, monitoring, and warning methods, relatively limited research has examined how drowsiness-induced low alertness affects behavior when they are interacting with other road users (Liu et al., 2022). Instead, most existing studies have focused on observable operational performance, investigating whether reduced alertness leads to degraded control quality and how such degradation is manifested. For example, in a driving simulation study, Guo et al. (2016) examined the relationship between driver drowsiness and reaction ability, and found that accumulated drowsiness can significantly prolong drivers' reaction time to abrupt hazards. Using on-road closed-loop track experiments, Cai et al. (2021) found that sleep deprivation led to more frequent lane departures and a higher risk of near-crash events. In a driving simulation study, Marando et al. (2022) further demonstrated that the combined effects of time on task, sleep deprivation, and circadian rhythm can impair speed control stability and overall driving performance. Taken together, these studies suggest that the effects of reduced alertness are not confined to a single driving operation, but can be reflected across multiple aspects of driving behavior, including reaction ability, lateral control, and speed regulation.

2.2. Driver alertness and CF performance

Table 1 summarizes existing empirical studies on the effects of reduced alertness, or increased drowsiness, on driving behavior. Overall, previous studies have mainly relied on three types of experimental platforms: driving simulators, on-road field experiments, and naturalistic driving data. Simulator studies allow drowsiness to be induced and driving scenarios to be standardized under safe, controlled, and repeatable conditions. However, their simplified

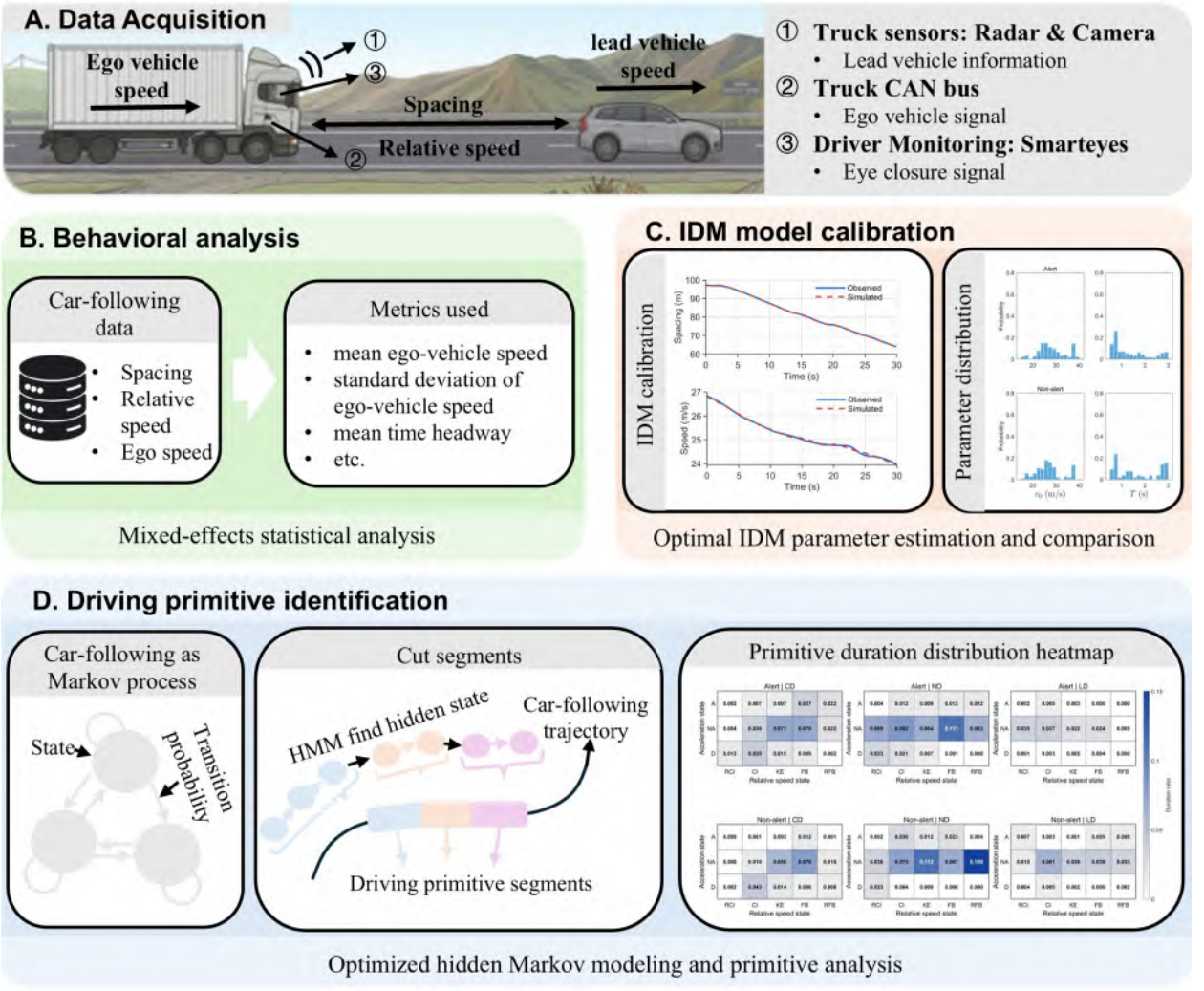


Figure 1: Overview of the study.

traffic environments, predetermined LV behavior, and relatively short driving exposure may limit the generalizability of the observed responses. Controlled on-road studies provide greater ecological validity, but routes, tasks, and exposure durations are still commonly specified by researchers. Naturalistic driving studies capture drowsiness and driving behavior during real-world operations, although they provide less experimental control and have generally focused on aggregate safety outcomes or safety-critical events rather than specific CF mechanisms.

Comparisons across vehicle types and research platforms suggest that drowsiness-related CF findings are not entirely consistent. Simulator studies with passenger cars generally report reduced headway safety, greater longitudinal-control variability, and increased rear-end crash risk under experimentally induced drowsiness (Thiffault and Bergeron, 2003; Ting et al., 2008; Filtness et al., 2012; Anund et al., 2017). Field studies with passenger cars also indicate changes in headway selection, but the direction and magnitude of these changes varied because drivers can adapt their behavior to actual traffic conditions (Philip et al., 2005; Hallvig et al., 2014; Zhang et al., 2016; Koopmans et al., 2023). In contrast to passenger cars, simulator evidence suggests more heterogeneous responses among truck drivers, with some drivers increasing their headway as a compensatory strategy while others exhibit riskier following behavior (Afghari et al., 2022). Finally, unlike findings from simulator studies, naturalistic truck studies have rarely examined drowsiness-related changes in specific CF variables, despite they captured substantially longer driving exposure and more realistic freight operations (Zhang et al., 2016; Mahajan and Velaga, 2021; Afghari et al., 2022; Chen et al., 2016).

These divergent findings in previous studies may be explained by differences in drowsiness-induction and classification methods, driving-exposure duration, traffic and LV control, drivers' professional experience, and the distinct braking, acceleration, and operational characteristics of passenger cars and heavy trucks.

Therefore, although previous research generally indicates that drowsiness can impair longitudinal driving safety, direct empirical evidence remains limited regarding how professional truck drivers modify their CF behavior under naturally occurring reduced-alertness states during long-distance operations.

2.3. Temporal modeling of CF behaviors

From a sequential modeling perspective, CF behavior should not be regarded as a static response, but rather as a stochastic dynamic process characterized by state transitions (Pariota et al., 2016; Ngoduy et al., 2019; Zhao et al., 2021). Previous research has constructed two-dimensional Markov state transition models based on the relationships between vehicle dynamics and CF decisions, thereby providing a theoretical foundation for the subsequent HMM-based approaches to analyze continuous CF behavior (Shi et al., 2016; Qu et al., 2017). Building on this foundation, an increasing number of studies have begun to employ driving primitives or behavioral semantics to characterize CF behavior at a finer level of granularity. For example, Wang et al. (2018) used naturalistic CF data and applied Bayesian nonparametric approaches, including hierarchical Dirichlet process hidden Markov model (HDP-HMM) (Teh et al., 2006), sticky hierarchical Dirichlet process hidden Markov model (sticky HDP-HMM) (Fox et al., 2007), and hierarchical Dirichlet process hidden semi-Markov model (HDP-HSMM) (Johnson and Willsky, 2013), to unsupervisedly extract primitive driving patterns from time-series data. These primitives were then semantically labeled according to drivers' physical and psychological perception thresholds, allowing the distribution of CF styles across drivers to be analyzed. Tang et al. (2025) further employed a Gaussian Mixture Model-Hidden Markov Model (GMM-HMM) (Juang, 1985) framework to decompose CF events in mixed traffic into driving primitives, in order to compare behavioral differences between human-driven vehicles and autonomous vehicles. Overall, existing studies suggest that primitive-based analysis can go beyond static statistical indicators and provide a more fine-grained characterization of the temporal structure of continuous CF behavior. However, such methods have so far been used mainly for general driving style identification, behavioral pattern segmentation, or mixed-traffic behavior comparison. Their application to explaining how CF behavior is temporally organized and evolves under different alertness conditions remains limited.

3. Data acquisition, description and pre-processing

3.1. Participants

Five male professional long-haul, heavy-duty truck drivers took part in the study (mean age = 42.6 years, SD = 3.9; 37–47 years). All participants held valid commercial freight licenses and were actively employed in an operating freight fleet. Drivers were selected based on current professional driving status and their ability and willingness to participate in the study. The study was carried out within a university–industry partnership. The study was approved by the Human and Artifacts Research Ethics Committee at the Hong Kong University of Science and Technology (Guangzhou) (No. HKUST(GZ)-HSP-2023-0013). In parallel, the collaborating company also conducted an internal review to ensure compliance with its operational safety requirements and data-governance framework. Prior to consent, each driver received a written consent form describing the research objectives, sensor modalities, and data handling procedures.

3.2. Route and driving task

The route is illustrated in Fig. 2, comprising a long-haul round trip between Wuxi, Jiangsu Province, and Qingdao, Shandong Province. A stop in Weifang was made during the return journey. In addition, some drivers made a stop in Linyi during the outbound journey. The average one-way distance was approximately 830 km, with a mean driving duration of 10.7 h. The itinerary consisted primarily of expressway/motorway segments representative of real-world long-haul freight operations. The route mainly followed major interprovincial expressway corridors in Jiangsu and Shandong. These roads generally provided two to four lanes per direction in different regions. Posted speed limits varied across road sections as well: while the regulatory maximum speed for heavy trucks was generally 100 km/h, the typical posted speed range for heavy vehicles along the route was approximately 80–100 km/h. The route crossed major passenger and freight corridors with generally moderate-to-high traffic demand. Publicly reported daily traffic volumes for representative sections of the G2 and G20 corridors were approximately 34,000–45,000 vehicles per day

Table 1
Summary of empirical studies on driver drowsiness and driving performance.

Study	Platform	Vehicle type	Participants	Drowsiness protocol	Driving exposure
Thiffault and Bergeron (2003)	Simulator	Passenger car	56 male drivers	Drowsiness induced by a monotonous road environment	80 min per driver
Ting et al. (2008)	Simulator	Passenger car	30 young male drivers	Drowsiness induced by continuous driving	90 min per driver
Filtness et al. (2012)	Simulator	Passenger car	39 male drivers	Sleep restriction condition compared with normal sleep condition	Approximately 4 h per driver
Anund et al. (2017)	Simulator	Passenger car	16 drivers, including 8 males	Daytime alert condition compared with nighttime/drowsy condition	Approximately 150–160 min per driver
Mahajan and Velaga (2021)	Simulator	Passenger car	50 male drivers	Partial sleep deprivation (PSD), including baseline, one night of PSD, and two consecutive nights of PSD	90–105 min per driver
Afghari et al. (2022)	Simulator	Truck	35 truck drivers; approximately 82.7% male	Naturally occurring drowsiness related to shift work, sleep loss, and circadian factors; no controlled sleep deprivation	Up to 15 min per trial
Philip et al. (2005)	Field study	Passenger car	22 male drivers	Sleep restriction condition compared with non-sleep-restricted condition	Approximately 20 h per driver
Hallvig et al. (2014)	Field study	Passenger car	33 drivers	Nighttime driving used to induce drowsiness	Approximately 180 min per driver
Zhang et al. (2016)	Field study	Passenger car	40 professional taxi drivers	Drowsiness induced by prolonged real-world driving	At least 6 h per driver
Chen et al. (2016)	Naturalistic driving study	Truck	96 commercial truck drivers	No controlled drowsiness induction; naturally occurring drowsiness inferred from real-world sleep and work-rest patterns	Approximately 4 weeks per driver
Marando et al. (2022)	Simulator	Passenger car	21 drivers, including 10 females	Total sleep deprivation for 62 h in a controlled laboratory, with repeated assessments at different times of day	30 min per trial, repeated every 8 h
Koopmans et al. (2023)	Simulator and field study	Passenger car	24 healthy male drivers	Randomized crossover comparison between a well-rested condition and one night of full sleep deprivation	Approximately 30 min of simulator driving and 30 min of on-road driving per assessment
Orsini et al. (2024)	Simulator	Passenger car	37 drivers; 73% male	Driving drowsiness associated with circadian disruption and sleep curtailment caused by the transition to daylight saving time	Three 50-min trials per driver; a subset completed two additional trials
Gaspar et al. (2025)	Simulator	Passenger car	90 drivers	Overnight driving following partial sleep restriction and extended wakefulness; self-initiated breaks were permitted	A 150-mile nighttime simulated highway drive per driver

Note. PSD = partial sleep deprivation. Naturalistic studies observe drivers during real-world operations without intentional drowsiness induction.

and more than 40,000 vehicles per day, respectively (Jiangsu Publicity News, 2023; Shandong Publicity Network, 2020). Note that these are the general traffic backgrounds of the corridors rather than the traffic volume measured during individual experimental trips, as continuous section-level traffic volumes were not available. Given that low-speed congested and stop-and-go conditions (i.e., lower than 20 m/s) were excluded during data preprocessing, the CF segments retained for analysis primarily represented uninterrupted and relatively stable expressway traffic. In accordance with local regulations, drivers were required to take a 15-min rest break at service areas approximately every 4 h of continuous driving.

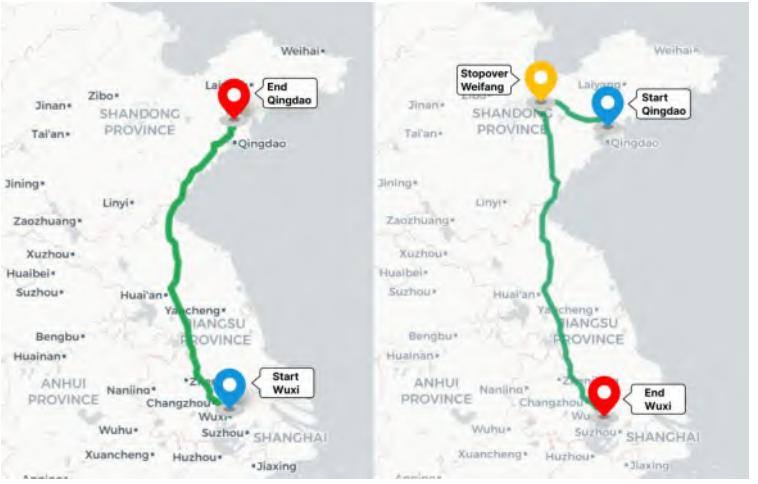


Figure 2: Driving route overview.

3.3. Apparatus

The experimental platform used in this study was a JAC K7 heavy-duty truck tractor equipped with the PlusAI assisted driving system and fitted with a standard cargo container. The overall vehicle configuration and experimental platform are illustrated in Fig. 3a. To comprehensively capture vehicle operational status and the surrounding traffic environment, the test vehicle was equipped with an onboard perception system, mainly including cameras and LiDAR sensors. These sensors were used to collect real-time information on the forward roadway, surrounding traffic participants, and road environment during driving; however, the assisted driving system was not engaged throughout the drives in the dataset. Inside the cab, a Smart Eye eye-tracking system was installed, as shown in Fig. 3b, to continuously record the driver's eye-movement behavior during vehicle operation, providing data for subsequent driver alertness assessment. As this study mainly focused on differences in CF behavior between alert and non-alert driver states under highway driving conditions, to ensure scene consistency and the validity of the analysis, data preprocessing excluded the small amount of data collected on non-highway segments.



(a) Truck platform used in the naturalistic driving experiment.



(b) SmartEye device inside the truck.

Figure 3: Experimental vehicle and in-cabin SmartEye setup.

3.4. CF Segment Extraction

The extraction of CF segments followed criteria reported in prior studies, thereby ensuring scenario consistency. Each extracted CF segment was non-overlapping, contained no shared samples, and was temporally separated from the adjacent extracted segments; each segment was therefore treated as an independent observational unit:

- The LV and the ego-vehicle need to be in the same lane throughout the data extraction period to ensure a continuous CF segment (Wen et al., 2022).
- The LV is within 130 m of the ego-vehicle to ensure that the behavior of the ego-vehicle can be affected by the LV (Seo et al., 2015).
- The duration of each CF segment was 30 s to balance the reliability of the CF data, the validity of eye-tracking data for alertness labeling (Wang et al., 2022; Trutschel et al., 2011), and the sample size.
- In addition, CF segments with ego-vehicle speeds lower than 20 m/s were excluded to remove stop-and-go traffic (Standing Committee of the National People's Congress, 2021). Another reason to remove such low-speed CF segments was that they constitute only a very small portion of the dataset.

3.5. Labeling alertness based on eye-tracking data

In this study, eyelid-closure data collected by the Smart Eye eye-tracking system were used as the ground truth for defining levels of alertness. The proportion of time during which the eyes remain closed within a fixed temporal window is calculated to obtain PERCLOS, which was used in this study as an ocular indicator of alertness level. Missing or invalid PERCLOS values caused by temporary loss of valid eye-tracking signals were handled using linear interpolation to maintain the continuity of the alertness estimation. According to (Grace and Steward, 2001) and (Blanco et al., 2009), a driver was considered to be in an alert state when PERCLOS is below 0.08; a moderately drowsy state when PERCLOS lies between 0.08 and 0.14; and a drowsy state when PERCLOS exceeds 0.14. The distribution of PERCLOS values across the analyzed CF segments is presented in Fig. 4

As shown in Table A1, a supplementary three-level analysis indicated that the moderately drowsy and drowsy groups generally exhibited changes in the same direction relative to the alert group. Most key measures did not differ significantly between the moderately drowsy and drowsy groups. Moreover, one of the five drivers contributed no drowsy segments, while two drivers contributed only two and three segments, respectively. Consequently, separate inference for the drowsy group could be unstable and the moderately drowsy and drowsy categories were combined into a non-alert category for our analysis.

This binary classification reduced class imbalance and provided a more statistically robust basis for the comparative analysis. Overall, a 30-s PERCLOS window and a threshold of 0.08 were adopted, resulting in 175 alert and 77 non-alert segments. Sensitivity analyses using alternative thresholds from 0.070 to 0.090 showed that the directions of the key findings were generally unchanged (Table A2), supporting the use of 0.08 as a relatively robust threshold for our primary analysis.

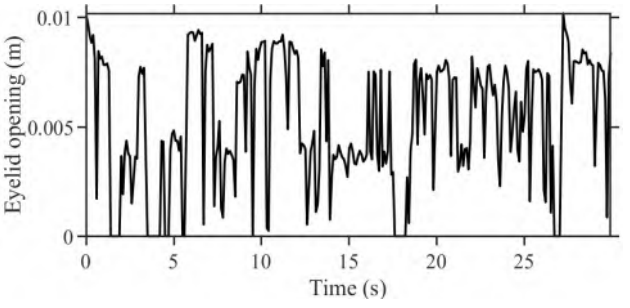


Figure 4: Distribution of PERCLOS values across the analyzed CF segments.

3.6. Trajectory filtering

To improve data quality, we applied a generic vehicle-speed trend filter designed by Zhu et al. (2024) to the raw speed signals, thereby suppressing noise and abnormal fluctuations prior to subsequent analysis. This filter can

essentially be described as an optimization process with decision variables, cost functions, and constraints. Specifically, a trend filter is a piecewise-polynomial smoothing method that denoises a signal by penalizing high-order differences, thereby preserving sharp changes while producing a smooth underlying trend. The decision variables here are the acceleration sequence

$$\boldsymbol{A} = [a(0),\, a(1),\, \ldots,\, a(n)]^T$$

where n denotes the total number of frames and $a(k)$ denotes the vehicle's acceleration at time step $k\Delta T$, with $\Delta T = T_n/n = 1/f_s$. In the equation, f_s is the sampling frequency of the synchronized data sequence, and T_n is the total traveling time.

The cost function is

$$C_2(\eta) = \frac{1}{2}\left\|A - A_{data}\right\|_2^2 + \lambda \left\|DA\right\|_1$$

In the equation, the input acceleration sequence is denoted by $A_{\text{data}} = \left[a_{\text{data}}(0),\, a_{\text{data}}(1),\, \ldots,\, a_{\text{data}}(n-1)\right]^{\top}$, where $a_{\text{data}}(i)$ represents the observed acceleration at the i_{th} moment. While $A = \left[a(0),\, a(1),\, \ldots,\, a(n-1)\right]^{\top}$ and represents the enhanced acceleration sequence that is to be estimated. The nonnegative regularization parameter λ controls the trade-off between the smoothness of the optimization variable and the magnitude of the data-fitting residual. Here, $\|\cdot\|_2$ denotes the Euclidean norm. D is a second-order finite difference operator.

$$D = \begin{bmatrix} 1 & -2 & 1 & & & & \\ & 1 & -2 & 1 & & & \\ & & \ddots & \ddots & \ddots & & \\ & & & 1 & -2 & 1 & \\ & & & & 1 & -2 & 1 \end{bmatrix}$$

The constraints are

$$-8 \le a(k) \le 5, \qquad v(k+1) - v(k) = \Delta T\, a(k), \qquad a(k+1) - a(k) \;\; = \Delta T\, j(k).$$

One example of the filtered vehicle speed is shown in Fig. 5. It can be observed that the random fluctuations in the speed signal are effectively suppressed after filtering, while the original variation trend is preserved. This improves the smoothness of the signal and provides more stable data support for subsequent vehicle-state analysis and driving behavior feature extraction.

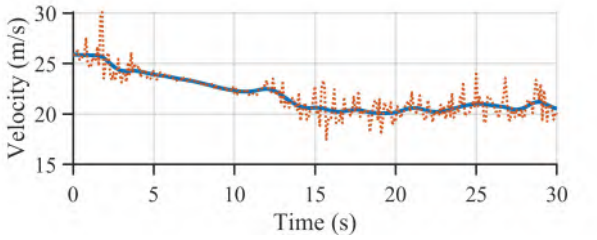


Figure 5: Representative raw and filtered velocity signals (blue: filtered, orange: raw).

4. CF behavior modeling and analyses

First, high-level behavioral indicators were used to compare CF characteristics between alert and non-alert conditions, thereby identifying overall differences in observable behaviors. Then, the Intelligent Driver Model (IDM) (Treiber et al., 2000) was introduced to provide a parameterized analysis of CF behavior, revealing potential differences in gap regulation, speed adaptation, and longitudinal control preferences. Finally, a primitive-level representation was further adopted to provide a fine-grained characterization of continuous CF behavior. Specifically, a disentangled sticky hierarchical Dirichlet process hidden Markov model (DS-HDP-HMM) (Zhou et al., 2020) was employed for unsupervised segmentation and structured modeling in order to identify potential differences in temporal behavioral patterns across alertness conditions.

4.1. Driving behavior indicators

For each CF segment, three longitudinal time-series variables were extracted, namely spacing s (bumper-to-bumper distance between LV and ego-vehicle), ego-vehicle speed v_e, and relative speed Δv. Relative speed was defined as the speed of the LV minus the speed of the ego-vehicle, i.e., $\Delta v = v_l - v_e$, where v_l denotes the LV speed and v_e denotes the ego-vehicle speed. Based on these variables, following previous studies (Mahajan and Velaga, 2021; Aramrattana et al., 2022), eight indicators were constructed to characterize the CF behavior, including mean ego-vehicle speed μ_{v_e}, standard deviation of ego-vehicle speed σ_{v_e}, standard deviation of spacing σ_s, mean time headway μ_{THW}, mean spacing μ_s, mean relative speed $\mu_{\Delta v}$, standard deviation of relative speed $\sigma_{\Delta v}$, and mean negative acceleration μ_{a^-}. Assuming that a CF segment contains N valid samples, these indicators are defined as follows:

$$\mu_{v_e} = \frac{1}{N}\sum_{i=1}^{N} v_{e,i} \tag{1}$$

$$\sigma_{v_e} = \sqrt{\frac{1}{N-1}\sum_{i=1}^{N}\left(v_{e,i} - \mu_{v_e}\right)^2} \tag{2}$$

$$\sigma_s = \sqrt{\frac{1}{N-1}\sum_{i=1}^{N}\left(s_i - \mu_s\right)^2} \tag{3}$$

$$\mu_s = \frac{1}{N}\sum_{i=1}^{N} s_i \tag{4}$$

$$THW_i = \frac{s_i}{v_{e,i}}, \qquad v_{e,i} > 0 \tag{5}$$

$$\mu_{THW} = \frac{1}{N}\sum_{i=1}^{N} THW_i \tag{6}$$

$$\mu_{\Delta v} = \frac{1}{N}\sum_{i=1}^{N} \Delta v_i \tag{7}$$

$$\sigma_{\Delta v} = \sqrt{\frac{1}{N-1}\sum_{i=1}^{N}\left(\Delta v_i - \mu_{\Delta v}\right)^2} \tag{8}$$

$$\mu_{a^-} = \frac{1}{N_-}\sum_{i:\,a_i<0} a_i \tag{9}$$

where, s_i is the longitudinal spacing between the ego-vehicle and the LV at sample i; $v_{e,i}$ is the ego-vehicle speed at sample i; Δv_i is the relative speed at sample i; and μ_s is the mean spacing within a CF segment. THW_i represents the time headway at sample i. N_- denotes the number of observations with negative acceleration.

These indicators capture longitudinal CF control behavior from multiple aspects. Specifically, μ_{v_e} and μ_{THW} reflect the driver's speed selection and safety-spacing preference, respectively; σ_{v_e} and σ_s characterize the stability of speed

regulation, distance maintenance, and safety margin control; and $\mu_{\Delta v}$ and $\sigma_{\Delta v}$ describe the overall trend and fluctuation of the dynamic interaction between the ego-vehicle and the LV.

It should be noted that the time-to-collision (TTC) (Hayward, 1972), commonly used as an indicator of CF risk, was not adopted, as no samples with $TTC < 5$ s were observed in our study, indicating that the recorded CF segment was generally within a relatively safe range (Vogel, 2003b). Moreover, given that excessively high THW values often correspond to non-typical CF conditions in which the LV exerts weak constraint on the ego-vehicle, to ensure that the retained samples adequately represented the constraints of the LV on the ego-vehicle, an upper bound was imposed on THW, and samples with $THW > 10$ s were excluded (Vogel, 2002). Potential differences between alert and non-alert driving states were identified through statistical comparisons of the above CF indicators. For all CF indicators except mean ego-vehicle speed, linear mixed-effects models were fitted with driver alertness state as the main fixed effect and ego-vehicle speed as a covariate. For mean ego-vehicle speed, driver alertness state was included as the only explanatory variable. In all models, driver-specific random intercepts were specified to account for repeated observations within the same driver.

4.2. Intelligent driver model

To characterize differences in CF behaviors under different alertness states, we then employed the classical IDM (Treiber et al., 2000) to describe real-world CF strategies. As a widely used microscopic CF model in traffic flow research, the IDM can effectively represent drivers' longitudinal acceleration and deceleration decisions. The model is expressed as:

$$a_e = a\left[1 - \left(\frac{v}{v_0}\right)^{\delta} - \left(\frac{s^*(v,\Delta v)}{s}\right)^2\right] \tag{10}$$

where

$$s^*(v,\Delta v') = s_0 + vT + \frac{v\Delta v'}{2\sqrt{ab}}, \qquad \Delta v' = v_e - v_l. \tag{11}$$

In the above equations, a_e denotes the ego-vehicle acceleration, v denotes the ego-vehicle speed, s denotes the spacing to the LV, and $\Delta v'$ denotes the relative speed, defined as the ego-vehicle speed minus the LV speed. The term $s^*(v,\Delta v)$ represents the desired dynamic spacing. The parameter δ is the acceleration exponent and was fixed at 4 according to previous studies (Treiber and Kesting, 2012).

We focused on the five IDM parameters with clear behavioral interpretations, namely the desired speed v_0, desired time headway T, minimum spacing s_0, maximum acceleration a, and comfortable deceleration b. Specifically, v_0 reflects the driver's preference for traffic operating efficiency; T and s_0 jointly represent the driver's preferred safety spacing and risk tolerance; a characterizes acceleration responsiveness and proactive CF tendency; and b reflects braking style. The IDM parameters were calibrated for each valid CF segment and then grouped according to alert and non-alert states for further statistical comparison. Specifically, linear mixed-effects models were employed to examine the effects of driving state (alert vs. non-alert) on the calibrated IDM parameters, with driving state specified as the fixed effect, each calibrated IDM parameter as the dependent variable, and a random intercept of the driver included.

4.3. HMM-based driving primitive modeling for CF behavior

Different HMM-based models differ in state-number specification, persistence constraints, and duration modeling, which may further affect segmentation performance and the interpretability of the extracted driving primitives. Accordingly, several HMM-based models, as described below, were adopted as the candidate models in this study. In this study, all HMM-based models were used to perform unsupervised segmentation of continuous CF episodes so as to extract latent driving primitives with greater heterogeneity and behavioral interpretability.

To reduce the influence of weakly supported or potentially redundant latent states, a minimum state-occupancy threshold was applied, because very short or rare primitives may provide limited semantic information and models may generate redundant states that affect interpretability and inference. Specifically, any identified latent state accounting for less than 2% of the total samples was excluded from subsequent analysis (Wang et al., 2020).

4.3.1. GMM-HMM

The GMM-HMM (Juang, 1985) represents the continuous CF process as a latent state sequence and its temporal transition process, as illustrated in Fig. 6a. In the model, $x_1, x_2, \ldots, x_T$ denote the latent state sequence over time, where different latent states correspond to different underlying CF behavior patterns, and $y_1, y_2, \ldots, y_T$ denote the observation vectors at each time step.

Let the observation sequence be defined as

$$\mathbf{y}_{1:T} = \{y_t\}_{t=1}^{T}, \qquad y_t = [s_t,\ v_t,\ \Delta v_t]^\top, \tag{12}$$

and the corresponding latent state sequence as

$$\mathbf{x}_{1:T} = \{x_t\}_{t=1}^{T}, \qquad x_t \in \{1, 2, \ldots, K\}, \tag{13}$$

where K is the number of latent states. The state transition probability is given by

$$P(x_t = j \mid x_{t-1} = i) = a_{ij}, \tag{14}$$

where a_{ij} denotes the probability of transitioning from state i to state j.

Conditioned on the latent state $x_t = k$, the emission probability of the observation is modeled by a Gaussian mixture distribution:

$$p(y_t \mid x_t = k) = \sum_{m=1}^{M} c_{k,m}\, \mathcal{N}(y_t \mid \mu_{k,m}, \Sigma_{k,m}), \tag{15}$$

where M is the number of mixture components, $c_{k,m}$ is the weight of the m-th Gaussian component, and $\mu_{k,m}$ and $\Sigma_{k,m}$ are the corresponding mean vector and covariance matrix, respectively.

Because GMM-HMM is a finite-state model, the number of latent states must be specified in advance. The Bayesian Information Criterion (BIC) was used for model selection:

$$BIC = -2 \ln L + p \ln N, \tag{16}$$

where L is the maximum likelihood, p is the number of model parameters, and N is the sample size. Based on the BIC results, $K = 6$ was selected as the optimal number of latent states for GMM-HMM.

4.3.2. Sticky HDP-HMM

The sticky HDP-HMM (Fox et al., 2007) is a Bayesian nonparametric HMM for modeling the dynamic transition process among latent states in CF behavior. As shown in Fig. 6b, the model uses the global state weights β to generate the local transition distribution π_i for each latent state, and combines the state-specific emission parameters θ_i to model the observation sequence. In this way, the model can adaptively learn the latent behavioral states and their transition structure without pre-specifying the number of states.

The generative process of the sticky HDP-HMM can be written as

$$\beta \sim GEM(\gamma), \tag{17}$$

$$\theta_i \sim H(\lambda), \qquad i = 1, 2, \ldots, \tag{18}$$

$$\pi_i \sim DP\left(\alpha + \kappa, \frac{\alpha\beta + \kappa\delta_i}{\alpha + \kappa}\right), \qquad i = 1, 2, \ldots, \tag{19}$$

$$x_t \mid x_{t-1} \sim \pi_{x_{t-1}}, \qquad t = 1, 2, \ldots, T, \tag{20}$$

$$y_t \mid x_t \sim F(\theta_{x_t}), \qquad t = 1, 2, \ldots, T. \tag{21}$$

Here, β denotes the global state weight distribution and follows a GEM (Griffiths–Engen–McCloskey) distribution, with γ being the concentration parameter. π_i denotes the transition probability distribution associated with state i. α controls the variability of the local transition distribution relative to the global distribution β. κ is the sticky parameter used to increase the self-transition tendency of state i, and δ_i denotes a unit mass concentrated on state i. By introducing the self-persistence bias term into the transition prior, the sticky HDP-HMM encourages adjacent observations to remain in the same latent state, thereby better capturing temporally continuous and stage-wise driving patterns.

4.3.3. HDP-HSMM

The HDP-HSMM (Johnson and Willsky, 2013) further extends the HDP-based framework by explicitly modeling state duration, as shown in Fig. 6c. Instead of performing state transitions at every time step, the HDP-HSMM represents the observation sequence as a series of state segments, each associated with a latent state and its duration. It shares components with the previous HDP-based model, including the global state weights, local transition distributions, state-specific emission parameters, and the observation emission process, which are not repeated here. The main difference between the HDP-HSMM and the HDP-based model lies in the introduction of the segment-level latent state z_s and its duration d_s:

$$z_s \mid z_{s-1} \sim \pi_{z_{s-1}}, \qquad s = 1, 2, \ldots, \tag{22}$$

$$d_s \sim g(\omega_{z_s}), \tag{23}$$

$$x_t = z_s, \qquad t = \tau_s, \tau_s + 1, \ldots, \tau_s + d_s - 1, \tag{24}$$

where z_s denotes the latent state associated with the s-th behavioral segment, d_s denotes the duration of that segment, $g(\omega_{z_s})$ is the duration distribution corresponding to state z_s, and τ_s is the starting time of the s-th segment. Thus, the HDP-HSMM no longer solely relies on self-transition tendencies to implicitly represent state persistence, but directly models the length of each state segment. This formulation reduces the occurrence of extremely short state fragments and improves the temporal interpretability of the segmentation results.

4.3.4. DS-HDP-HMM

The DS-HDP-HMM (Zhou et al., 2020) extends the sticky HDP-HMM by disentangling state persistence from the transition structure among states. As shown in Fig. 6d, in the sticky HDP-HMM, the stickiness parameter is directly coupled with the transition distribution π_j, whereas in the DS-HDP-HMM the probability of remaining in the current state and the probability of transitioning to another state are modeled separately. The components shared with the sticky HDP-HMM, including the global state weights, the state-specific emission parameters, and the observation emission process, are not repeated here.

The main difference between the DS-HDP-HMM and the sticky HDP-HMM is that the local transition distribution in DS-HDP-HMM is reformulated as a non-self-transition distribution $\bar{\pi}_j$, and the state-specific persistence parameter κ_j is introduced as follows, together with the auxiliary variable w_t:

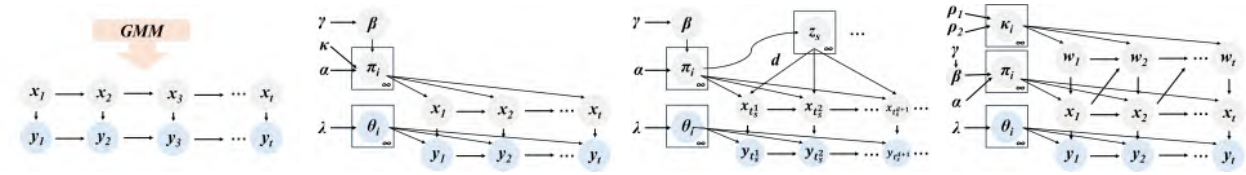
$$\bar{\pi}_j \sim DP(\alpha, \beta), \qquad j = 1, 2, \ldots, \tag{25}$$

$$\kappa_j \sim \text{Beta}(\rho_1, \rho_2), \qquad j = 1, 2, \ldots, \tag{26}$$

$$w_t \mid x_{t-1} = j \sim \text{Bernoulli}(\kappa_j), \qquad t = 2, \ldots, T, \tag{27}$$

$$x_t = \begin{cases} x_{t-1}, & w_t = 1, \\ \tilde{x}_t, \quad \tilde{x}_t \sim \bar{\pi}_{x_{t-1}}, & w_t = 0, \end{cases} \tag{28}$$

where $\bar{\pi}_j$ denotes the non-self-transition distribution associated with state j, κ_j denotes the persistence probability of state j, and ρ_1 and ρ_2 are the Beta prior parameters. The auxiliary variable w_t indicates whether the latent state at time t remains the same as that at time $t-1$. When $w_t = 1$, the current state is retained; when $w_t = 0$, the system transitions according to $\bar{\pi}_{x_{t-1}}$. Accordingly, the DS-HDP-HMM no longer uses a single sticky term to implicitly control state persistence. This formulation allows the model to characterize both the persistence tendency of each latent state and the cross-state transition structure more flexibly, thereby providing a finer representation of the complex temporal evolution of CF behavior.



(a) GMM-HMM (b) sticky HDP-HMM (c) HDP-HSMM (d) DS-HDP-HMM

Figure 6: Graphical models of the four HMM-based approaches.

5. Results and Discussions

5.1. Macroscopic behavioral metrics

The comparison of CF behavior metrics between alert and non-alert states is summarized in Table 2. The results showed that among the examined CF features, the μ_{THW} and μ_s differed significantly between alert and non-alert states, with a significantly higher μ_{THW} observed in the non-alert state. No statistical differences ($p > .05$) were found for the other features.

Given that the intraclass correlation coefficient of μ_{THW} was 0.220, indicating that approximately 22.0% of the total variance could be attributed to between-driver differences, additional robustness analyses were conducted. After including driver as a fixed effect, μ_{THW} remained significantly higher in the non-alert state ($\beta = 0.457$ s, $p = 0.0030$; Table 3), with an effect estimate comparable to that of the main analysis without including the driver as a fixed effect. The leave-one-driver-out sensitivity analysis further showed that the estimated effect remained positive in all models (Table A3). These results indicate that the increase in μ_{THW} under the non-alert state cannot be explained solely by individual CF styles.

Further, the μ_{THW} is generally regarded as an indicator of CF conservativeness and preference for safety margin, with a larger value indicating that the driver maintained a greater temporal buffer for responding to LV deceleration. In the present study, the mean inter-vehicle spacing, μ_s, was significantly larger in the non-alert state, whereas neither the mean ego-vehicle speed nor the mean negative acceleration differed significantly between the alert and non-alert states. These results indicate that the increase in μ_{THW} was primarily associated with a larger spacing to the LV, rather than changes in overall speed preference or deceleration intensity. This pattern is consistent with a more conservative spacing strategy, whereby drivers with reduced alertness maintained a greater temporal safety margin under relatively stable highway CF conditions. Such an adjustment may serve as a compensatory response to the potential risks associated with reduced alertness and is similar to the longitudinal behavioral adaptations observed under distracted driving conditions (Choudhary and Velaga, 2017). However, it is still possible that drivers could fail to follow the acceleration of LVs passively with reduced alertness. Future research may validate these two explanations by comparing the paces of the speed adjustments of the LV and the ego-vehicle.

Note that our finding of larger time headway differs from previous passenger-car CF studies. Zhang et al. (2016) and Mahajan and Velaga (2021) both reported that drowsiness led to shorter THW and higher CF risk. In contrast, the present study found a significantly larger mean THW in the non-alert state, while no significant differences were observed for the other CF indicators. This suggests that, under naturalistic highway CF scenarios, truck drivers were

more likely to enlarge the temporal safety margin to the LV to compensate for their impaired alertness, potentially because of their increased experience and risk awareness. This interpretation is also consistent with a simulator study Afghari et al. (2022), which reported that most drivers increased headway under drowsy conditions.

Table 2
Comparison of CF features between alert and non-alert states.

Feature	Alert (Mean ± SD)	Non-alert (Mean ± SD)	Statistic	p-value	ICC
μ_{v_e}	23.73 ± 1.83	23.33 ± 1.72	$F(1, 250.00) = 2.6185$	0.107	≈ 0
σ_{v_e}	0.57 ± 0.47	0.52 ± 0.51	$F(1, 250.00) = 0.5697$	0.451	≈ 0
σ_s	9.18 ± 7.47	8.98 ± 7.16	$F(1, 250.00) = 0.0376$	0.846	≈ 0
μ_s	67.58 ± 27.08	78.89 ± 27.65	$F(1, 247.16) = 7.8540$	0.005*	0.2214
μ_{THW}	2.85 ± 1.17	3.38 ± 1.19	$F(1, 247.16) = 10.1051$	0.002*	0.2197
μ_{THW} adjusted for μ_{v_e}	2.85 ± 1.17	3.38 ± 1.19	$F(1, 246.23) = 9.0721$	0.003*	0.2217
$\mu_{\Delta v}$	−0.50 ± 1.21	−0.43 ± 1.22	$F(1, 250.00) = 0.1724$	0.678	≈ 0
$\sigma_{\Delta v}$	0.57 ± 0.41	0.50 ± 0.41	$F(1, 250.00) = 1.6484$	0.200	≈ 0
μ_{a^-}	−0.09 ± 0.09	−0.09 ± 0.07	$F(1, 242.00) = 0.5070$	0.477	≈ 0

Note: μ_{v_e} denotes mean ego-vehicle speed; σ_{v_e} denotes the standard deviation of ego-vehicle speed; σ_s denotes the standard deviation of inter-vehicle spacing; μ_s denotes mean inter-vehicle spacing; μ_{THW} denotes mean time headway; $\mu_{\Delta v}$ denotes mean relative speed; $\sigma_{\Delta v}$ denotes the standard deviation of relative speed; and μ_{a^-} denotes mean negative acceleration. Group values are reported as raw mean ± standard deviation (SD). ICC denotes the intraclass correlation coefficient obtained from the null model. ICC values equal to or numerically close to zero are reported as ≈ 0. * $p < 0.05$.

Table 3
Robustness of the non-alert state effect on mean time headway to driver-specific differences.

Outcome	Driver specification in the model	Estimate	95% CI	p-value
μ_{THW}	Driver as random effect	0.4815	[0.1832, 0.7799]	0.0017*
	Driver as fixed effects	0.4798	[0.1811, 0.7785]	0.0018*
μ_{THW} adjusted for μ_{v_e}	Driver as random effect	0.4589	[0.1588, 0.7590]	0.0029*
	Driver as fixed effects	0.4569	[0.1564, 0.7574]	0.0030*

Note: Estimates represent the difference between the non-alert and alert states (non-alert minus alert). Positive estimates indicate a longer mean time headway in the non-alert state. Random-intercept models account for between-driver variation through (1|Driver), whereas driver-fixed-effects models control for stable differences among individual drivers. * $p < 0.05$.

5.2. IDM-based CF performance analysis

5.2.1. Model calibration and evaluation metrics

Examples of IDM fitting results are illustrated in Fig. 7. The root mean square error (RMSE) and the correlation coefficient (R) were further used to assess the fitting quality. For a variable x (e.g., speed v or spacing s), the RMSE is defined as:

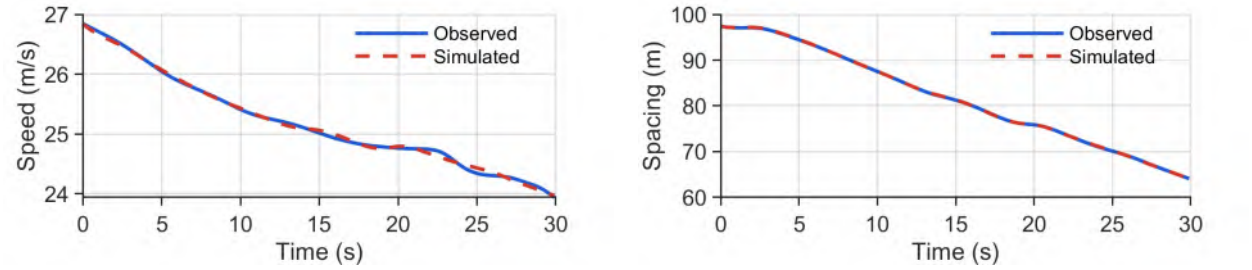
$$\text{RMSE}_x = \sqrt{\frac{1}{N}\sum_{i=1}^{N}\left(x_i^{\text{sim}} - x_i^{\text{obs}}\right)^2}, \tag{29}$$

where x_i^{sim} and x_i^{obs} denote the simulated and observed values at time step i, respectively, and N is the segment length. The correlation coefficient R, which measures the consistency in variation trends between the simulated and observed sequences, is defined as:

$$R_x = \frac{\sum_{i=1}^{N}\left(x_i^{\text{obs}} - \bar{x}^{\text{obs}}\right)\left(x_i^{\text{sim}} - \bar{x}^{\text{sim}}\right)}{\sqrt{\sum_{i=1}^{N}\left(x_i^{\text{obs}} - \bar{x}^{\text{obs}}\right)^2}\sqrt{\sum_{i=1}^{N}\left(x_i^{\text{sim}} - \bar{x}^{\text{sim}}\right)^2}}, \tag{30}$$

where $\bar{x}^{obs}$ and $\bar{x}^{sim}$ are the mean values of the observed and simulated sequences, respectively. The average RMSE for speed fitting reached 0.198 m/s, with an average correlation coefficient R of 0.928; whereas the average RMSE for spacing fitting was 0.702 m, with an average R of 0.984, comparable to previous CF studies (e.g., RMSE values of 0.41 m/s for speed reported by Gunter et al. (2019)), indicating that the IDM achieved good performance for reconstructing both speed and spacing in CF segments.

Particle swarm global optimization was performed with multiple independent searches, and a paired moving-block residual bootstrap was used to evaluate the stability of the parameter estimates. For each trajectory, three independent searches were conducted, with the parameters randomly initialized within $v_0 \in [15, 40]$ m/s, $T \in [0.5, 3.0]$ s, $a \in [0.2, 4.0]$ m/s^2, $b \in [0.5, 4.5]$ m/s^2, and $s_0 \in [0.5, 8.0]$ m, while δ was fixed at 4. The solution with the lowest objective function value was retained as the final estimate. Across the 252 trajectories, the median bootstrap refitting success rate was 100%. The relative differences in the objective function values obtained from different random initializations were extremely small, with a median of 3.58×10^{-11} and a 90th percentile of 1.52×10^{-7}, indicating that the independent searches converged to nearly identical optimal fits. Of the 252 trajectories, 249 produced at least two near-optimal solutions and were therefore included in the parameter-dispersion analysis; the remaining three had only one qualifying solution. Among the 249 trajectories with multiple near-optimal solutions, the median standardized parameter dispersion was only 6.75×10^{-6}, with a 90th percentile of 4.54×10^{-4}, showing that solutions with similar fitting performance also yielded highly consistent parameter estimates. Overall, no concerns of local-optimum or parameter-instability were observed under the adopted calibration settings.



(a) Speed comparison.

(b) Spacing comparison.

Figure 7: Examples of IDM reproducing CF segments.

5.2.2. Comparison of IDM-related CF parameters

As shown in Table 4 and Fig. 8, differences in the fitted IDM parameters between the alert and non-alert states were further examined. Specifically, the IDM comfortable deceleration parameter b was significantly lower in the non-alert state, with an intraclass correlation coefficient (ICC) close to zero (indicating that there were no detectable stable differences in the mean parameter values across drivers), and the direction of the effect consistent across the leave-one-driver-out analyses (Table A3, suggesting that this difference may not be attributed only to between-driver heterogeneity or to any single driver). However, the actual mean negative acceleration, μ_{a^-}, did not differ significantly between the two alertness states (Table 2). This indicates that the lower calibrated b was not accompanied by a corresponding change in observed deceleration intensity. Taken together, these findings suggest that reduced alertness was associated with a lower comfortable deceleration setting in the calibrated CF model, reflecting a shift in longitudinal control preference rather than systematically milder or stronger actual braking behavior.

5.3. Primitive-level temporal structure analysis

5.3.1. Variable segmentation and threshold selection

The IDM only describes static CF strategies. To evaluate temporal characteristics of the CF strategies, we further mapped three physically meaningful CF semantics, namely relative distance, relative speed, and longitudinal acceleration, to primitives. These variables were then discretized into several categorical levels based on the distributional characteristics of the observed data. Detailed definitions of the variable categories, abbreviations, and threshold intervals are provided in Table 5, while the rationale and procedure for threshold determination are illustrated in Fig. 9, with reference to prior studies (Zou et al., 2022; Wang et al., 2018) and the characteristics of the current dataset.

Table 4
Comparison of calibrated CF model parameters between alert and non-alert states.

Feature	Alert (Mean ± SD)	Non-alert (Mean ± SD)	Statistic	p-value	ICC
v_0	28.7673 ± 5.1869	27.7648 ± 5.0057	$F(1, 250) = 2.0403$	0.154	≈ 0
T	1.2182 ± 0.7172	1.3891 ± 0.7923	$F(1, 250) = 3.0134$	0.084	0.0733
a	1.1384 ± 1.0994	1.0585 ± 1.0402	$F(1, 250) = 0.2917$	0.590	≈ 0
b	3.1727 ± 1.2868	2.8154 ± 1.3666	$F(1, 250) = 3.9687$	0.047*	≈ 0
s_0	3.8437 ± 2.2296	4.0713 ± 2.0604	$F(1, 250) = 0.5831$	0.446	≈ 0

Note: v_0 denotes desired speed, T denotes desired time headway, a denotes maximum acceleration, b denotes comfortable deceleration, and s_0 denotes minimum spacing. Adjusted ICC denotes the intraclass correlation coefficient obtained from the adjusted mixed-effects model. ICC values smaller than 0.001 are reported as ≈ 0. * $p < 0.05$.

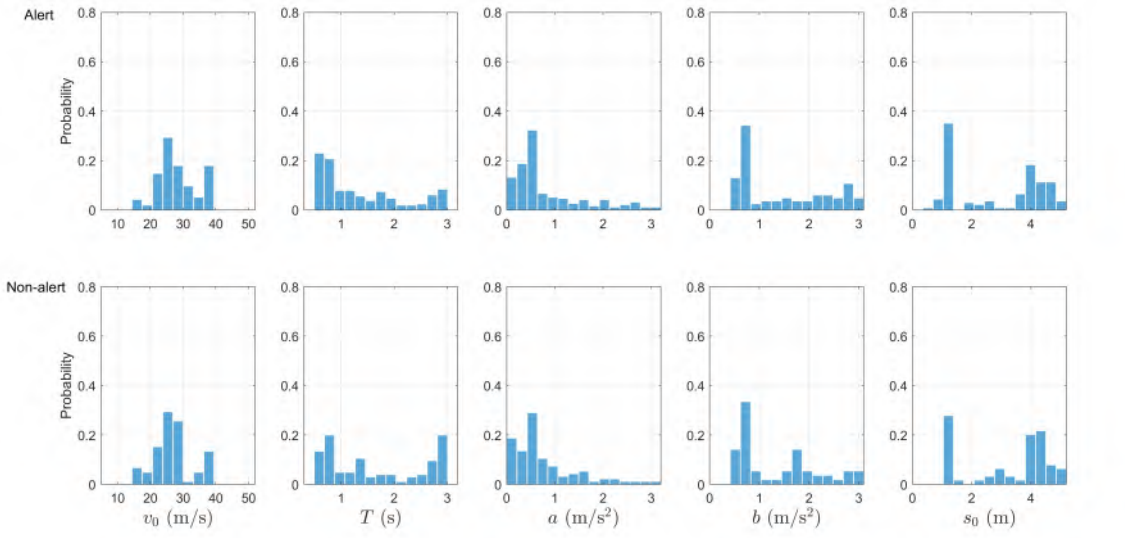
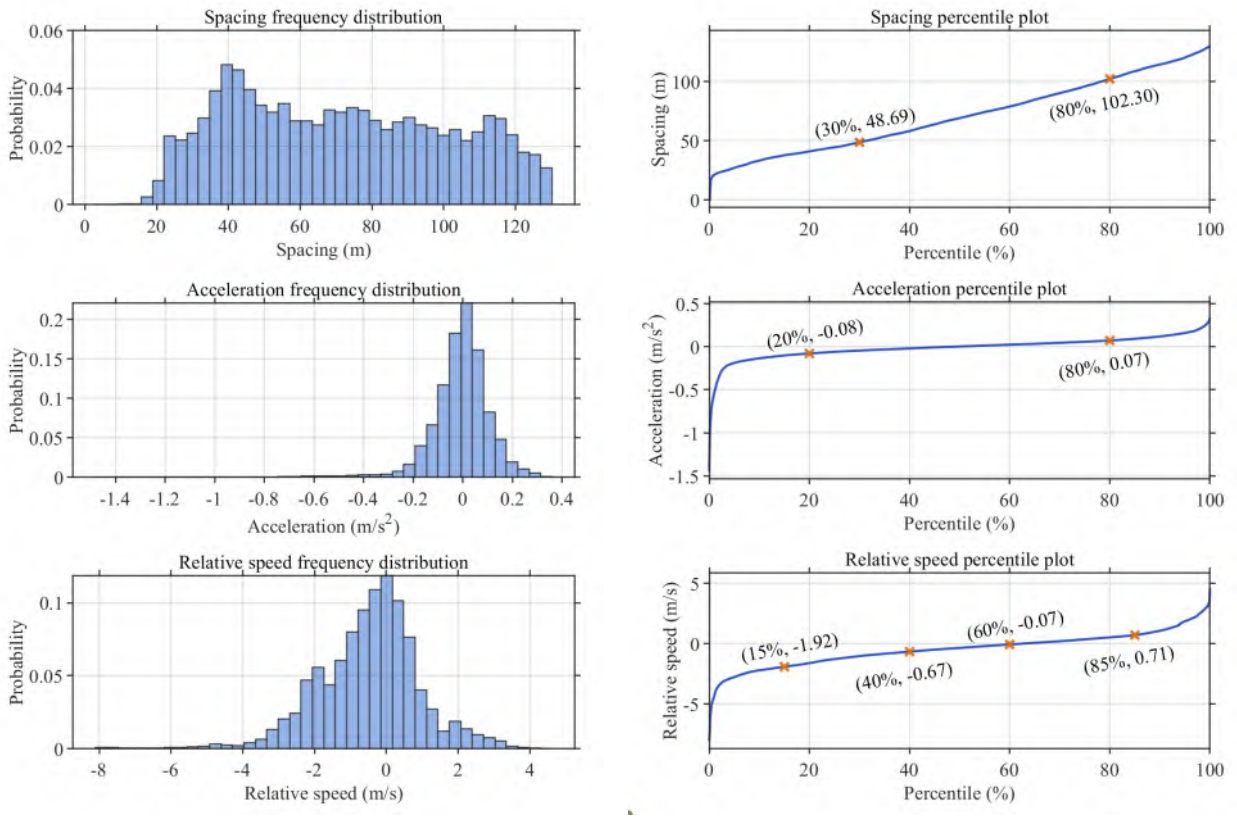


Figure 8: Distribution of calibrated IDM parameters under alert and non-alert states.

Table 5
Variable segmentation based on percentile-derived thresholds.

Variable	Variable state	Threshold
Relative distance (m)	Long distance (LD)	> 102.30
	Normal distance (ND)	(48.69, 102.30]
	Close distance (CD)	(5, 48.69]
Relative speed (m/s)	Rapid gap opening (RGO)	> 0.71
	Gap opening (GO)	$(-0.07, 0.71]$
	Keeping (KE)	$(-0.67, -0.07]$
	Closing in (CI)	$(-1.92, -0.67]$
	Rapidly closing in (RCI)	≤ -1.92
Longitudinal acceleration (m/s^2)	Acceleration (A)	> 0.07
	No acceleration (NA)	$(-0.08, 0.07]$
	Deceleration (D)	≤ -0.08



(a) The histogram of frequency distribution.

(b) Threshold values of three variables, with the definitions provided in Table 5

Figure 9: Distribution characteristics and threshold values of the CF-related variables

5.3.2. Comparisons of HMM models

As mentioned previously, to ensure that the identified behavioral primitives can adequately capture the dynamic variations of the CF process while preserving reasonable temporal continuity, four representative hidden Markov models were considered in this study.

Figure 10 compares the observed-data log likelihood per training sample during model training. The DS-HDP-HMM and Sticky HDP-HMM showed comparable training-fit performance. To further evaluate model generalizability, a leave-one-driver-out evaluation was conducted using the same data-processing procedure and input variables. In each evaluation round, one driver was designated as the independent test set, while data from all remaining drivers were used for model training. This procedure was repeated until each driver had served once as the test driver, and the overall model performance was summarized by averaging the results across all evaluation rounds. This driver-level split was used solely for model comparison; after model selection, all models were fitted to the complete dataset for the subsequent behavioral analysis. Each Bayesian model was run for 100 iterations, with the first 40 discarded as burn-in. The predictive log-likelihood per observation was then calculated on the test set, with larger values indicating better predictive performance on unseen data. Averaged across all leave-one-driver-out evaluation rounds, the DS-HDP-HMM achieved the highest predictive log likelihood (-1.18), outperforming the Sticky HDP-HMM (-1.29), HDP-HSMM (-1.44), and GMM-HMM (-2.75). These results indicate that the DS-HDP-HMM provided the best generalization performance in the independent test.

Further, as shown in Fig. 11, the segmentation results of a representative CF event reveal substantial differences among the four models. Compared with the alternative methods, DS-HDP-HMM achieved a more balanced distribution of CF primitive segments with different lengths. In other words, it was capable of capturing meaningful transition boundaries between adjacent primitives, while avoiding overly fragmented segmentation of the continuous driving

process. This characteristic makes the resulting primitives more consistent with the temporal evolution of real-world CF behavior and therefore more behaviorally interpretable.

This advantage is further supported by the duration statistics of primitive driving patterns for all CF events, as summarized in Table 6. Relative to the other candidate models, DS-HDP-HMM produced lower proportions of primitives with durations shorter than 1 s and equal to 30 s, indicating that it can effectively suppress unrealistic high-frequency switching while also avoiding excessive persistence of a single state. Further, the distribution of primitives with other durations (other than 1s or 30 s) was also more balanced, suggesting that the DS-HDP-HMM was able to preserve sensitivity to behavioral changes while more appropriately characterizing the natural temporal continuity of primitive driving patterns.

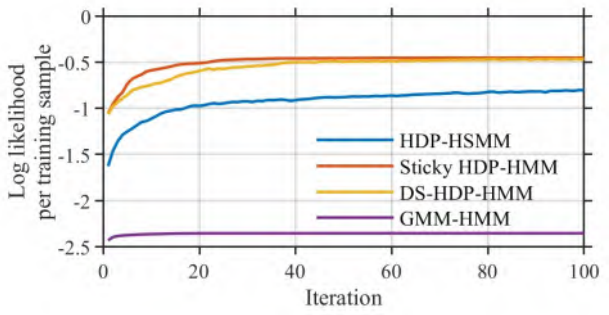


Figure 10: Log-likelihood per training sample over iterations for the four HMM-based models.

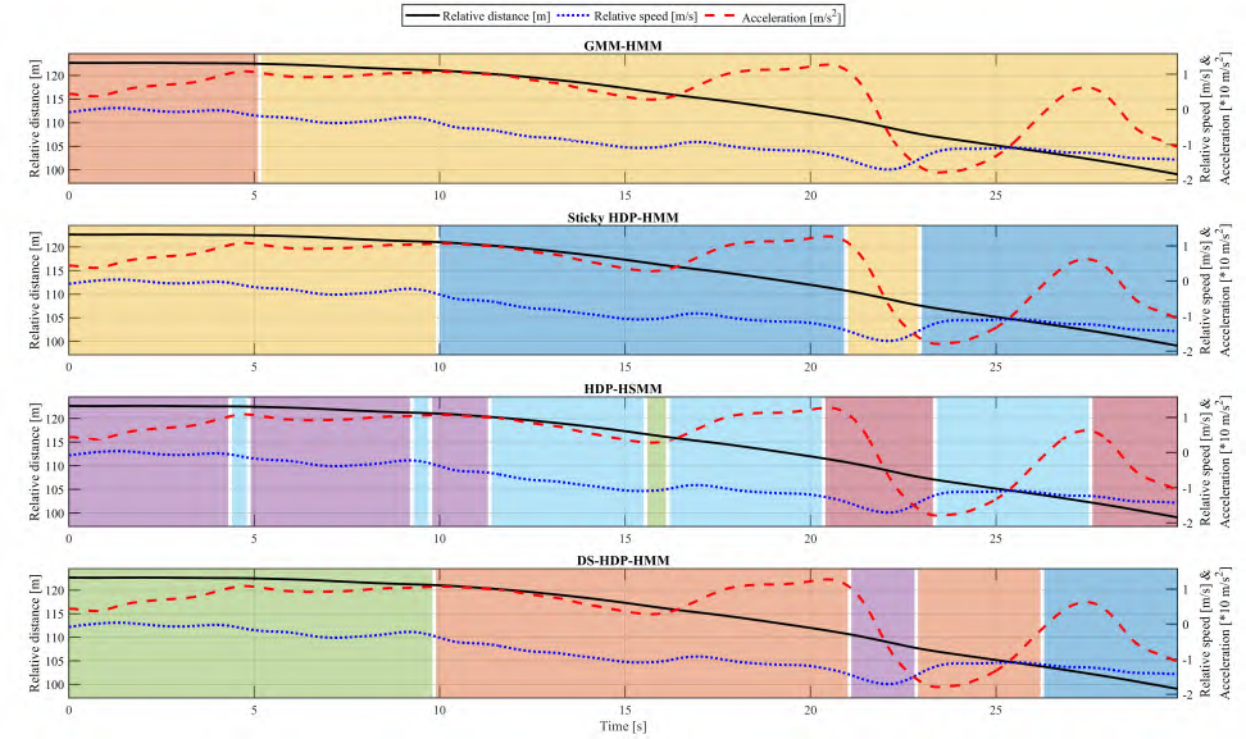


Figure 11: Representative example of CF primitive segmentation results produced by different HMM-based models.

It is worth noting that, as shown in Table 6, DS-HDP-HMM still identified the entire CF segment as a single primitive in a certain proportion of cases. This phenomenon should be interpreted in light of the specific driving

Table 6
The durations of the primitive driving pattern from the four models.

Model	The distribution of durations of primitive driving patterns							
	<1	$[1,5)$	$[5,10)$	$[10,15)$	$[15,20)$	$[20,25)$	$[25,30)$	$=30$
GMM-HMM	0.0167	0.1674	0.1778	0.1423	0.1318	0.1046	0.0481	0.2113
Sticky HDP-HMM	0.0841	0.2737	0.2283	0.1722	0.0921	0.0614	0.0240	0.0641
HDP-HSMM	0.3616	0.6384	0.0000	0.0000	0.0000	0.0000	0.0000	0.0000
DS-HDP-HMM	0.0752	0.3325	0.2550	0.1445	0.0870	0.0411	0.0153	0.0494

context considered in this study. The analyzed data consist of stable CF events under highway driving conditions, in which longitudinal vehicle motion was generally characterized by strong continuity and relatively limited fluctuations. Therefore, when no obvious behavioral state transition was observed within a given segment, it is reasonable for the model to identify the whole segment as a single primitive. Such a result is consistent with the actual characteristics of driving behavior and should not be regarded as evidence of insufficient segmentation capability. Further, Fig. 12 presents a comparative analysis of the kinematic characteristics associated with 30 s primitives and non-30 s primitives. The results indicate that the longitudinal acceleration and relative speed of the 30 s primitives are both predominantly distributed around zero, suggesting that the longitudinal interaction between the ego-vehicle and the LV was weak in these segments and that the overall CF process remained relatively stable. This finding supports the superior performance of DS-HDP-HMM in identifying some complete CF segments as a single primitive, and also indicates that the model is capable of preserving the genuinely long-duration behavioral patterns that existed in stable highway CF scenarios. Therefore, based on the above findings, the DS-HDP-HMM was selected for further analyses.

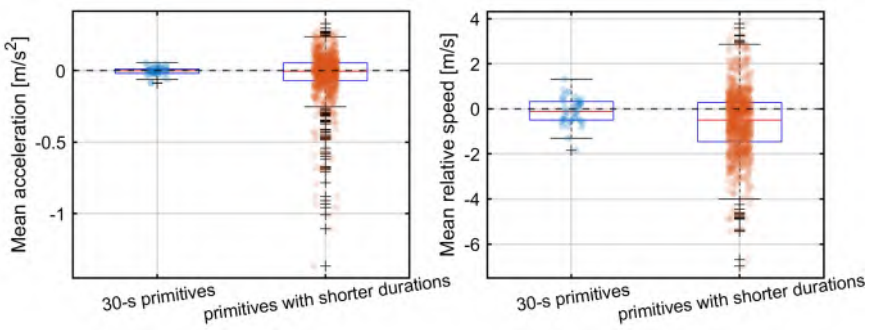


Figure 12: Comparison of mean acceleration and mean relative speed between 30-s primitives and primitives with shorter durations.

5.3.3. Comparisons of the CF behaviors with the HMM models

Based on the DS-HDP-HMM model, behavioral primitives were extracted from each CF segment, and distributions of primitive driving patterns with different durations were then summarized, as shown in Fig. 13. Overall, the CF behavior in the non-alert segment was more stable and conservative. Specifically, non-alert drivers tended to adopt a near-constant longitudinal control mode, where active and continuous speed adjustments were less frequent. Compared with alert CF segments, the proportion of NA-related primitives increased in the non-alert segments, with this tendency being particularly evident in the KE, GO, and RGO relative-speed states, indicating that non-alert drivers remained for longer periods in a behavioral mode characterized by weak longitudinal control input, while the spacing to the LV was maintained or gradually enlarged. Further, the proportions of A and D-related primitives generally decreased in non-alert segments, suggesting that drivers' active response to the motion of the LV was weakened and that longitudinal regulation became more delayed and passive. Further, non-alert drivers were more likely to accept the current or even slightly enlarged CF spacing and maintain vehicle operation in a relatively smooth manner. This tendency was

particularly evident under the LD and ND conditions, where a large proportion of non-alert primitives was concentrated in the NA-KE, NA-GO, and NA-RGO regions.

Table 7 shows that the mean durations of the CF primitives generally increased in the non-alert segments, although statistically significant differences were observed only for the RCI and A primitives. Specifically, non-alert drivers remained in the rapidly closing in and acceleration states for longer durations, suggesting that reduced alertness may prolong dynamic longitudinal adjustment processes and delay the termination of approaching or accelerating behaviors. No significant differences were found for the remaining relative-distance, relative-speed, or longitudinal-acceleration primitives, indicating that reduced alertness primarily affected the persistence of specific dynamic CF states without substantially altering the overall temporal structure of the primitives.

In summary, the results shown in Fig. 13 indicate that highway CF behavior with a low level of alertness is characterized by a greater preference for larger time gaps, weaker longitudinal regulation intensity, and stronger behavioral persistence. The significantly longer durations of the RCI and acceleration A primitives further suggest that reduced alertness prolonged specific dynamic longitudinal adjustment processes, although the temporal structure of most other primitives remained unchanged. Compared with the alert drivers, non-alert drivers were more likely to maintain the CF process through less frequent but more persistent control actions, rather than through continuous active corrections. These tendencies reflect lower control activity and weaker closed-loop correction among non-alert drivers in stable highway CF scenarios, consistent with findings from lane-keeping studies showing that drowsy drivers tend to correct the steering wheel less frequently (Fairclough and Graham, 1999). These findings demonstrate that the primitive representation based on DS-HDP-HMM can effectively reveal the temporal differences in CF control strategies between alert and non-alert states.

These findings also provide implications for the design of warning systems for heavy-duty trucks. Previous studies on truck drivers' reactions to hazards have shown that forward collision warning systems should account for differences in driver behavior and real-time risk levels, and that previous negative or false warnings may influence drivers' responses to subsequent warnings (Shao et al., 2023, 2025). Combined with these findings, we suggest that warning strategies for heavy trucks could incorporate driver alertness and current CF behavior when determining warning timing and intensity, rather than relying solely on uniform thresholds.

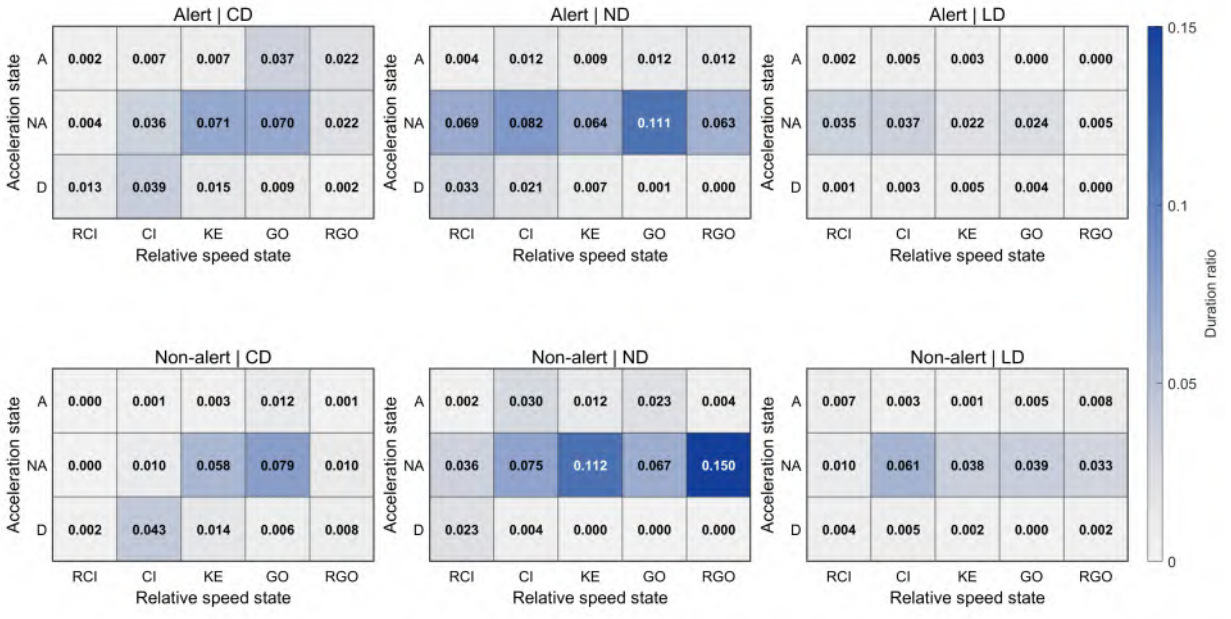


Figure 13: Heatmaps of the duration ratio of primitive driving patterns under different spacing states and driving conditions. Note: the abbreviations in the figure can be found in Table 5

Table 7
Comparison of primitive durations between alert and non-alert states.

Variable state	Primitive duration comparison between alert and non-alert states				
	Alert, mean ± SD	Non-alert, mean ± SD	F statistic	p	ICC
Relative distance					
Long distance (LD)	12.23 ± 9.30	13.65 ± 10.45	$F(1, 119) = 0.616$	0.434	≈ 0
Normal distance (ND)	9.81 ± 7.93	11.13 ± 7.42	$F(1, 374) = 2.197$	0.139	≈ 0
Close distance (CD)	6.11 ± 6.20	6.43 ± 5.83	$F(1, 349) = 0.162$	0.688	≈ 0
Relative speed					
Rapid gap opening (RGO)	8.73 ± 6.23	10.02 ± 8.68	$F(1, 119) = 0.886$	0.348	≈ 0
Gap opening (GO)	9.21 ± 9.16	10.34 ± 8.45	$F(1, 197) = 0.574$	0.449	0.066
Keeping (KE)	9.07 ± 9.31	10.32 ± 9.43	$F(1, 157) = 0.557$	0.457	≈ 0
Closing in (CI)	7.87 ± 6.72	9.55 ± 7.01	$F(1, 230) = 2.945$	0.088	≈ 0
Rapidly closing in (RCI)	7.26 ± 5.72	11.59 ± 7.89	$F(1, 138) = 10.147$	0.002*	≈ 0
Longitudinal acceleration					
Acceleration (A)	5.04 ± 4.52	6.82 ± 5.66	$F(1, 159) = 4.027$	0.047*	≈ 0
No acceleration (NA)	10.85 ± 8.48	12.18 ± 8.65	$F(1, 502) = 2.573$	0.109	≈ 0
Deceleration (D)	5.33 ± 5.30	5.86 ± 5.17	$F(1, 184) = 0.312$	0.577	≈ 0

6. Limitations and future work

This study mainly focused on CF behaviors of long-haul truck drivers; therefore, the applicability of the findings to other road environments and among other types of drivers needs to be further examined. Moreover, because the limited and unevenly distributed low-speed segments were excluded, the present findings mainly apply to relatively stable, high-speed highway CF conditions and may not generalize to congested or stop-and-go traffic. In addition, time of day, traffic conditions, and LV characteristics could not be fully controlled in this naturalistic study and may have introduced confounding. Therefore, the findings should be interpreted within the highway CF conditions represented in the dataset. Moreover, the effects of some IDM-related parameters, such as the comfortable deceleration parameter b and acceleration duration, were not consistently significant under different PERCLOS thresholds, indicating that these parameters may be sensitive to alertness-label definitions and should be interpreted cautiously.

Future work could extend the analysis to a wider range of road types and traffic conditions and identify behavioral features or model parameters that are more sensitive and robust to alertness. On this basis, it may be possible to develop alertness-monitoring detection methods based on CF behavioral characteristics, enabling autonomous vehicles to identify the states of surrounding human drivers and adopt adaptive interaction strategies for different drivers. At the same time, as a preliminary study, we included a limited number of truck drivers. Future research should expand the dataset to further validate our findings. Finally, accelerator-pedal position, brake-pedal operation, and braking frequency were not recorded in the naturalistic driving dataset. Therefore, the primitive-level findings could not be cross-validated using independent vehicle-control indicators. Future research should collect these variables to further examine whether the observed primitive distributions directly reflect changes in longitudinal control activities.

7. Conclusions

This study first established and publicized one of the first CF datasets for long-haul truck drivers. Then, we investigated the differences in highway CF behavior between alert and non-alert heavy-duty truck drivers using the naturalistic driving data. From the perspectives of high-level behavioral indicators, model-based CF parameters, and primitive-level temporal structure, the results consistently showed that reduced alertness was associated with changes

in drivers' longitudinal adjustment patterns, which may partly reflect compensatory responses. Specifically, drivers in a non-alert state not only preferred a more conservative spacing strategy, but also adopted a milder and less aggressive longitudinal adjustment pattern. The primitive-level analyses further explained the difference in overall CF metrics and IDM parameters: under the non-alert condition, drivers remained in near-constant and weak-regulation patterns for longer periods, while active acceleration and deceleration corrections became less frequent. These findings have deepened the understanding of the longitudinal control mechanism of non-alert driving in real-world highway environments and provided useful behavioral evidence to support the design of longitudinal control strategies in intelligent driving assistance systems to cope with non-alert road users.

8. Appendix

Table A1
Three-level sensitivity analysis results for selected CF measures.

Measure	Alert (Mean ± SD)	Moderately drowsy (Mean ± SD)	Drowsy (Mean ± SD)	Mixed-effects model p, Moderate vs. Drowsy
Mean THW (s)	2.8528 ± 1.1662	3.1959 ± 1.1412	3.8424 ± 1.2015	0.039
IDM b (m/s^2)	3.173 ± 1.287	2.764 ± 1.437	2.943 ± 1.194	0.607
RCI duration (s)	7.2643 ± 5.7170	11.6810 ± 7.7103	11.1000 ± 10.0863	0.896
Acceleration duration (s)	5.0426 ± 4.5202	6.6133 ± 6.0722	7.5111 ± 4.2025	0.682

Note. The reported p-values compare the moderately drowsy and drowsy groups using linear mixed-effects models with driver-specific random intercepts.

Table A2
Sensitivity analyses of key findings to alternative PERCLOS thresholds

Outcome	PERCLOS threshold	Alert, mean ± SD	Non-alert, mean ± SD	Difference	Mixed-effects model p
Mean time headway, μ_{THW} (s)	0.070	2.822 ± 1.125	3.206 ± 1.237	0.365	0.014
	0.075	2.830 ± 1.155	3.285 ± 1.208	0.408	0.005
	0.080	2.853 ± 1.166	3.381 ± 1.188	0.482	0.002
	0.085	2.899 ± 1.167	3.373 ± 1.221	0.435	0.008
	0.090	2.919 ± 1.168	3.355 ± 1.243	0.396	0.019
IDM comfortable deceleration, b (m/s^2)	0.070	3.198 ± 1.288	2.865 ± 1.347	−0.333	0.049
	0.075	3.166 ± 1.297	2.865 ± 1.346	−0.302	0.085
	0.080	3.173 ± 1.287	2.815 ± 1.367	−0.357	0.047
	0.085	3.140 ± 1.300	2.856 ± 1.358	−0.284	0.130
	0.090	3.111 ± 1.302	2.915 ± 1.372	−0.197	0.312
Rapidly closing-in duration, RCI (s)	0.070	6.878 ± 5.584	10.564 ± 7.207	3.686	0.001
	0.075	7.212 ± 5.706	10.819 ± 7.620	3.607	0.004
	0.080	7.264 ± 5.717	11.588 ± 7.893	4.324	0.002
	0.085	7.331 ± 5.757	11.818 ± 8.029	4.487	0.002
	0.090	7.482 ± 5.834	12.331 ± 8.509	4.849	0.004
Acceleration duration, A (s)	0.070	4.870 ± 4.485	7.029 ± 5.471	2.159	0.011
	0.075	5.043 ± 4.520	6.821 ± 5.657	1.778	0.047
	0.080	5.043 ± 4.520	6.821 ± 5.657	1.778	0.047
	0.085	5.065 ± 4.619	6.997 ± 5.488	1.932	0.039
	0.090	5.169 ± 4.747	6.655 ± 5.191	1.486	0.118

Note. Summary statistics are reported as mean ± SD. Difference represents the estimated non-alert minus alert contrast. Positive values indicate higher parameter values or longer primitive durations in the non-alert state, whereas negative values indicate lower values in the non-alert state. Mixed-effects models included alertness state as a fixed effect and driver as a random intercept. The PERCLOS threshold of **0.080** was used in the primary analysis. THW = time headway; RCI = rapidly closing in; A = acceleration; SD = standard deviation.

Table A3

Leave-one-driver-out sensitivity analysis of key findings

Outcome	Analysis scenario	Alert n	non-alert n	Alert, mean ± SD	Non-alert, mean ± SD	Difference
Mean time headway, μ_{THW} (s)	Full sample	175	77	2.853 ± 1.166	3.381 ± 1.188	+0.528
	Exclude driver 1	122	40	2.785 ± 1.196	3.169 ± 1.225	+0.384
	Exclude driver 2	154	67	2.883 ± 1.195	3.421 ± 1.202	+0.538
	Exclude driver 3	132	61	2.668 ± 1.065	3.281 ± 1.189	+0.613
	Exclude driver 4	135	71	2.946 ± 1.193	3.358 ± 1.227	+0.412
	Exclude driver 5	157	69	2.951 ± 1.154	3.575 ± 1.082	+0.624
IDM comfortable deceleration, b (m/s^2)	Full sample	175	77	3.173 ± 1.287	2.815 ± 1.367	−0.357
	Exclude driver 1	122	40	3.145 ± 1.313	2.626 ± 1.399	−0.519
	Exclude driver 2	154	67	3.183 ± 1.289	2.916 ± 1.327	−0.268
	Exclude driver 3	132	61	3.290 ± 1.209	2.794 ± 1.388	−0.496
	Exclude driver 4	135	71	3.030 ± 1.341	2.855 ± 1.364	−0.175
	Exclude driver 5	157	69	3.208 ± 1.271	2.806 ± 1.367	−0.402
Rapidly closing-in duration, RCI (s)	Full sample	115	25	7.264 ± 5.717	11.588 ± 7.893	+4.324
	Exclude driver 1	86	5	6.866 ± 5.614	10.900 ± 5.672	+4.034
	Exclude driver 2	97	22	6.941 ± 5.760	11.746 ± 8.063	+4.804
	Exclude driver 3	85	25	7.892 ± 5.797	11.588 ± 7.893	+3.696
	Exclude driver 4	84	25	7.495 ± 5.630	11.588 ± 7.893	+4.093
	Exclude driver 5	108	23	7.198 ± 5.740	11.587 ± 8.240	+4.389
Acceleration duration, A (s)	Full sample	122	39	5.043 ± 4.520	6.821 ± 5.657	+1.778
	Exclude driver 1	96	24	4.888 ± 4.426	5.758 ± 4.448	+0.871
	Exclude driver 2	106	36	5.082 ± 4.443	6.958 ± 5.779	+1.876
	Exclude driver 3	93	29	5.222 ± 4.519	6.897 ± 5.830	+1.675
	Exclude driver 4	96	34	5.069 ± 4.539	7.041 ± 5.935	+1.972
	Exclude driver 5	97	33	4.956 ± 4.691	7.149 ± 5.845	+2.193

Note. Summary statistics are reported as mean ± SD. Difference represents the non-alert minus alert contrast. Positive values indicate higher parameter values or longer primitive durations in the non-alert state, whereas negative values indicate lower values in the non-alert state. For each sensitivity analysis, one driver was excluded, and the summary statistics were recalculated using data from the remaining four drivers. Sample sizes for RCI and A differ from those for mean THW and b because only observations containing the corresponding driving primitive were included. THW = time headway; IDM = Intelligent Driver Model; RCI = rapidly closing in; A = acceleration; SD = standard deviation.

References

Afghari, A.P., Papadimitriou, E., Pilkington-Cheney, F., Filtness, A., Brijs, T., Brijs, K., Cuenen, A., De Vos, B., Dirix, H., Ross, V., et al., 2022. Investigating the effects of sleepiness in truck drivers on their headway: An instrumental variable model with grouped random parameters and heterogeneity in their means. Analytic methods in accident research 36, 100241.

Anund, A., Fors, C., Ahlstrom, C., 2017. The severity of driver fatigue in terms of line crossing: a pilot study comparing day-and night time driving in simulator. European transport research review 9, 31.

Aramrattana, M., Fu, J., Selpi, 2022. Behavioral adaptation of drivers when driving among automated vehicles. Journal of intelligent and connected vehicles 5, 309–315.

Blanco, M., Bocanegra, J.L., Morgan, J.F., Fitch, G.M., Medina, A., Olson, R.L., Hanowski, R.J., Daily, B., Zimmermann, R.P., Howarth, H.D., et al., 2009. Assessment of a drowsy driver warning system for heavy-vehicle drivers. Technical Report. U.S. Department of Transportation, National Highway Traffic Safety Administration.

Cai, A.W., Manousakis, J.E., Singh, B., Kuo, J., Jeppe, K.J., Francis-Pester, E., Shiferaw, B., Beatty, C.J., Rajaratnam, S.M., Lenné, M.G., et al., 2021. On-road driving impairment following sleep deprivation differs according to age. Scientific reports 11, 21561.

Casey, G.J., Miles-Johnson, T., Stevens, G.J., 2024. Heavy vehicle driver fatigue: Observing work and rest behaviours of truck drivers in australia. Transportation Research Part F: Traffic Psychology and Behaviour 104, 136–153.

Chang, L.Y., Mannering, F., 1999. Analysis of injury severity and vehicle occupancy in truck-and non-truck-involved accidents. Accident Analysis & Prevention 31, 579–592.

Chen, G.X., Fang, Y., Guo, F., Hanowski, R.J., 2016. The influence of daily sleep patterns of commercial truck drivers on driving performance. Accident Analysis & Prevention 91, 55–63.

Choudhary, P., Velaga, N.R., 2017. Mobile phone use during driving: Effects on speed and effectiveness of driver compensatory behaviour. Accident Analysis & Prevention 106, 370–378.

Duffy, J.F., Zitting, K.M., Czeisler, C.A., 2015. The case for addressing operator fatigue. Reviews of human factors and ergonomics 10, 29–78.

Fairclough, S.H., Graham, R., 1999. Impairment of driving performance caused by sleep deprivation or alcohol: a comparative study. Human factors 41, 118–128.

Filtness, A.J., Reyner, L.A., Horne, J.A., 2012. Driver sleepiness—comparisons between young and older men during a monotonous afternoon simulated drive. Biological psychology 89, 580–583.

Fox, E.B., Sudderth, E.B., Jordan, M.I., Willsky, A.S., 2007. The sticky HDP-HMM: Bayesian nonparametric hidden markov models with persistent states. Preprint / early technical report version.

Gaspar, J., Tefft, B., Carney, C., Horrey, W.J., 2025. The impact of self-initiated breaks during drowsy driving. Sleep 48, zsaf150.

Grace, R., Steward, S., 2001. Drowsy driver monitor and warning system, in: Driving Assessment Conference, University of Iowa. pp. 64–69.

Gunter, G., Stern, R., Work, D.B., 2019. Modeling adaptive cruise control vehicles from experimental data: model comparison, in: 2019 IEEE intelligent transportation systems conference (ITSC), IEEE. pp. 3049–3054.

Guo, M., Li, S., Wang, L., Chai, M., Chen, F., Wei, Y., 2016. Research on the relationship between reaction ability and mental state for online assessment of driving fatigue. International journal of environmental research and public health 13, 1174.

Hallvig, D., Anund, A., Fors, C., Kecklund, G., Åkerstedt, T., 2014. Real driving at night–predicting lane departures from physiological and subjective sleepiness. Biological psychology 101, 18–23.

Hayward, J.C., 1972. Near miss determination through use of a scale of danger. Highway Research Record , 24–34.

Hussain, Z., Mohammed, S.S., Dias, C., Hussain, Q., Alhajyaseen, W.K., 2025. Empirical analysis of car-following behavior: Impacts of driver demographics, leading vehicle types, and speed limits on driver behavior and safety. Transportation Research Part F: Traffic Psychology and Behaviour 108, 188–205.

Jiangsu Publicity News, 2023. Jiangsu expressway expansion projects enter an accelerated construction period. URL: https://www.zgjssw.gov.cn/yaowen/202307/t20230703_7995832.shtml. accessed 24 July 2026, in Chinese.

Johnson, M.J., Willsky, A.S., 2013. Bayesian nonparametric hidden semi-markov models. Journal of Machine Learning Research 14, 673–701.

Juang, B.H., 1985. Maximum-likelihood estimation for mixture multivariate stochastic observations of markov chains. AT&T Technical Journal 64, 1235–1249. doi:10.1002/j.1538-7305.1985.tb00273.x.

Kesting, A., Treiber, M., Helbing, D., 2010. Enhanced intelligent driver model to access the impact of driving strategies on traffic capacity. Philosophical Transactions of the Royal Society A: Mathematical, Physical and Engineering Sciences 368, 4585–4605.

Koopmans, I., Doll, R.J., van der Wall, H., de Kam, M., Groeneveld, G.J., Cohen, A., Zuiker, R., 2023. Fit for purpose of on-the-road driving and simulated driving: A randomised crossover study using the effect of sleep deprivation. PLoS one 18, e0278300.

Liu, F., Chen, D., Zhou, J., Xu, F., 2022. A review of driver fatigue detection and its advances on the use of rgb-d camera and deep learning. Engineering Applications of Artificial Intelligence 116, 105399.

Mabry, J.E., Camden, M., Miller, A., Sarkar, A., Manke, A., Ridgeway, C., Iridiastadi, H., Crowder, T., Islam, M., Soccolich, S., et al., 2022. Unravelling the complexity of irregular shiftwork, fatigue and sleep health for commercial drivers and the associated implications for roadway safety. International journal of environmental research and public health 19, 14780.

Mahajan, K., Velaga, N.R., 2021. Sleep-deprived car-following: Indicators of rear-end crash potential. Accident Analysis & Prevention 156, 106123.

Marando, I., Matthews, R.W., Grosser, L., Yates, C., Banks, S., 2022. The effect of time on task, sleep deprivation, and time of day on simulated driving performance. Sleep 45, zsac167.

McCartt, A.T., Rohrbaugh, J.W., Hammer, M.C., Fuller, S.Z., 2000. Factors associated with falling asleep at the wheel among long-distance truck drivers. Accident Analysis & Prevention 32, 493–504.

Ngoduy, D., Lee, S., Treiber, M., Keyvan-Ekbatani, M., Vu, H.L., 2019. Langevin method for a continuous stochastic car-following model and its stability conditions. Transportation Research Part C: Emerging Technologies 105, 599–610.

Orsini, F., Domenie, E.D., Zarantonello, L., Costa, R., Montagnese, S., Rossi, R., 2024. Long-term effects of daylight saving time on driving fatigue. Heliyon 10.

Pariota, L., Bifulco, G.N., Brackstone, M., 2016. A linear dynamic model for driving behavior in car following. Transportation Science 50, 1032–1042.

Philip, P., Sagaspe, P., Moore, N., Taillard, J., Charles, A., Guilleminault, C., Bioulac, B., 2005. Fatigue, sleep restriction and driving performance. Accident Analysis & Prevention 37, 473–478.

Qu, T., Yu, S., Shi, Z., Chen, H., 2017. Modeling driver's car-following behavior based on hidden markov model and model predictive control: A cyber-physical system approach, in: 2017 11th Asian Control Conference (ASCC), IEEE. pp. 114–119.

Ramsay, E., 2006. Management of traffic-related effects of heavy vehicles on urban freight corridors. Faculty of Built Environment and Engineering .

Seo, T., Kusakabe, T., Asakura, Y., 2015. Estimation of flow and density using probe vehicles with spacing measurement equipment. Transportation Research Part C: Emerging Technologies 53, 134–150.

Shandong Publicity Network, 2020. Shandong's expressway mileage to exceed 7,400 kilometers by the end of the year. URL: https://www.sdxc.gov.cn/jryw/snzdxw/202009/t20200928_11622227.htm. accessed 24 July 2026, in Chinese.

Shao, Y., Shi, X., Zhang, Y., Zhang, Y., Xu, Y., Chen, W., Ye, Z., 2023. Adaptive forward collision warning system for hazmat truck drivers: Considering differential driving behavior and risk levels. Accident Analysis & Prevention 191, 107221.

Shao, Y., Xu, Y., Ye, Z., Zhang, Y., Chen, W., Shiwakoti, N., Shi, X., 2025. Understanding the impacts of negative advanced driving assistance system warnings on hazardous materials truck drivers' responses using interpretable machine learning. Engineering Applications of Artificial Intelligence 146, 110308.

Shi, S., Lin, N., Zhang, Y., Cheng, J., Huang, C., Liu, L., Lu, B., 2016. Research on markov property analysis of driving cycles and its application. Transportation Research Part D: Transport and Environment 47, 171–181.

Standing Committee of the National People's Congress, 2021. Law of the people's republic of china on road traffic safety. National People's Congress of the People's Republic of China. URL: https://jtgl.beijing.gov.cn/jgj/jgxx/flfg/fl/205308/index.html. revised in 2021, Article 67.

Tang, S., Zou, Y., Wu, S., Xie, Y., Zhang, Y., 2025. Comparing car-following behavior patterns of human-driven vehicles and autonomous vehicles in a mixed traffic environment. IEEE Transactions on Intelligent Transportation Systems .

Teh, Y.W., Jordan, M.I., Beal, M.J., Blei, D.M., 2006. Hierarchical dirichlet processes. Journal of the American Statistical Association 101, 1566–1581. URL: http://www.jstor.org/stable/27639773.

Thiffault, P., Bergeron, J., 2003. Monotony of road environment and driver fatigue: a simulator study. Accident Analysis & Prevention 35, 381–391.

Ting, P.H., Hwang, J.R., Doong, J.L., Jeng, M.C., 2008. Driver fatigue and highway driving: A simulator study. Physiology & behavior 94, 448–453.

Tomson, M., Mathew, T.V., Velaga, N.R., 2025. A systematic review of studies investigating the impact of sleep deprivation on drivers' physiology and driving performance. Transportation Research Part F: Traffic Psychology and Behaviour 109, 458–479.

Treiber, M., Hennecke, A., Helbing, D., 2000. Congested traffic states in empirical observations and microscopic simulations. Physical review E 62, 1805.

Treiber, M., Kesting, A., 2012. Traffic flow dynamics: data, models and simulation. Springer Science & Business Media.

Trutschel, U., Sirois, B., Sommer, D., Golz, M., Edwards, D., 2011. Perclos: An alertness measure of the past, in: Driving Assessment Conference Archive, University of Iowa. pp. 172–179.

Vogel, K., 2002. What characterizes a "free vehicle" in an urban area? Transportation Research Part F: Traffic Psychology and Behaviour 5, 15–29. doi:10.1016/S1369-8478(02)00003-7.

Vogel, K., 2003a. A comparison of headway and time to collision as safety indicators. Accident analysis & prevention 35, 427–433.

Vogel, K., 2003b. A comparison of headway and time to collision as safety indicators. Accident Analysis & Prevention 35, 427–433. doi:10.1016/S0001-4575(02)00022-2.

Wang, K., Yang, Y., Wang, S., Shi, Z., 2022. Research on car-following model considering driving style. Mathematical Problems in Engineering 2022, 7215697.

Wang, W., Xi, J., Zhao, D., 2018. Driving style analysis using primitive driving patterns with bayesian nonparametric approaches. IEEE Transactions on Intelligent Transportation Systems 20, 2986–2998.

Wang, W., Zhang, W., Zhu, J., Zhao, D., 2020. Understanding v2v driving scenarios through traffic primitives. IEEE Transactions on Intelligent Transportation Systems 23, 610–619.

Wen, X., Cui, Z., Jian, S., 2022. Characterizing car-following behaviors of human drivers when following automated vehicles using the real-world dataset. Accident Analysis & Prevention 172, 106689.

Zainuddin, N.I., Arshad, A.K., Hamidun, R., Haron, S., Hashim, W., 2023. Influence of road and environmental factors towards heavy-goods vehicle fatal crashes. Physics and Chemistry of the Earth, Parts A/B/C 129, 103342.

Zhang, H., Wu, C., Yan, X., Qiu, T.Z., 2016. The effect of fatigue driving on car following behavior. Transportation research part F: traffic psychology and behaviour 43, 80–89.

Zhang, X., Sun, J., Qi, X., Sun, J., 2019. Simultaneous modeling of car-following and lane-changing behaviors using deep learning. Transportation research part C: emerging technologies 104, 287–304.

Zhao, L., Rilett, L., Haque, M.S., 2021. Hidden markov model of lane-changing-based car-following behavior on freeways using naturalistic driving data. Transportation research record 2675, 550–561.

Zhou, D., Gao, Y., Paninski, L., 2020. Disentangled sticky hierarchical dirichlet process hidden markov model, in: Joint European Conference on Machine Learning and Knowledge Discovery in Databases, Springer. pp. 612–627.

Zhu, F., Chang, C., Li, Z., Li, B., Li, L., 2024. A generic optimization-based enhancement method for trajectory data: Two plus one. Accident Analysis & Prevention 200, 107532.

Zou, Y., Zhu, T., Xie, Y., Zhang, Y., Zhang, Y., 2022. Multivariate analysis of car-following behavior data using a coupled hidden markov model. Transportation research part C: emerging technologies 144, 103914.